ceramics

MDPI

Communication

Metal Halide Perovskite Light-Emitting Transistor with Tunable Emission Based on Electrically Doped Semiconductor Nanocrystal-Based Microcavities

Francesco Scotognella

Department of Applied Science and Technology, Politecnico di Torino, Corso Duca degli Abruzzi 24, 10129 Torino, Italy; francesco.scotognella@polito.it

Abstract: Electroluminescence of metal halide perovskites has been widely reported via the fabrication and optimization of light-emitting diodes and light-emitting transistors. Light-emitting transistors are particularly interesting owing to the additional control of the gate voltage on the electroluminescence. In this work, the design of a microcavity, with a defect mode that can be tuned with an applied voltage, integrated with a metal halide light-emitting transistor is shown. The optical properties of the device have been simulated with the transfer matrix method, considering the wavelength-dependent refractive indexes of all the employed materials. The tunability of the microcavity has been obtained via the employment of doped semiconductor nanocrystalline films, which show a tunable plasma frequency and, thus, a tunable refractive index as a function of the applied voltage. Consequently, the tunability of the electroluminescence of the metal halide perovskite light-emitting transistor has been demonstrated.

Keywords: light-emitting transistors; metal halide perovskites; microcavities

check for updates

Citation: Scotognella, F. Metal Halide Perovskite Light-Emitting Transistor with Tunable Emission Based on Electrically Doped Semiconductor Nanocrystal-Based Microcavities. *Ceramics* **2023**, *6*, 1894–1899. https://doi.org/10.3390/ceramics6030116

Academic Editor: Gilbert Fantozzi

Received: 22 July 2023
Revised: 29 August 2023
Accepted: 7 September 2023
Published: 11 September 2023

1. Introduction

The electroluminescence of metal halide perovskites is attracting increasing attention owing to their narrowband emission, near-unity photoluminescence efficiency, and low-cost solution-based fabrication [1–5]. In addition to the manufacture of very efficient solar cells [6–10] and light-emitting diodes [11–13], the development of perovskite-based light-emitting transistors is of great interest [14–19].

To enhance the electroluminescence of light-emitting transistors, the integration of photonic crystals as gate dielectrics has been reported in organic light-emitting transistors. In this way, enhanced emission efficiency and enhanced emission directionality has been demonstrated [20,21]. Because of the similar wet chemistry fabrication techniques for organic semiconductors and metal halide perovskites, photonic crystals as gate dielectrics can also be implemented for metal halide perovskite light-emitting transistors. To further increase the enhancement, a combination of a metal halide perovskite light-emitting transistor with a microcavity has been proposed. In such a design, a photonic crystal is used as a gate dielectric and the other photonic crystal is fabricated onto the metal halide perovskite layer [22].

With a proper choice of materials, a microcavity can be tuned with an external stimulus in order to tune the light-emitting transistor emission. For example, the employment of metals or doped semiconductors [23–25] as components of the photonic crystal leads to a tunable photonic band gap with the application of an external voltage [26]. In this work, the design of a metal halide perovskite light-emitting transistor combined with a microcavity, which can be tuned with an external voltage, is presented. The transmission spectra are simulated with the transfer matrix method and the wavelength-dependent refractive indexes of all the materials have been employed.

2. Materials and Methods

The simulations of the light transmission spectra of the structures studied in this work have been performed with the transfer matrix method, which is well established for one-dimensional multilayer systems [27–30]. The studied system is glass/multilayer/air.

For silicon dioxide (SiO_2), the following Sellmeier equation has been employed [31,32]:

$$n^2_{SiO_2}(\lambda) - 1 = \frac{0.6961663\lambda^2}{\lambda^2 - 0.0684043^2} + \frac{0.4079426\lambda^2}{\lambda^2 - 0.1162414^2} + \frac{0.8974794\lambda^2}{\lambda^2 - 9.896161^2} \quad (1)$$

For titanium dioxide (TiO_2), the wavelength-dependent refractive index is given by [33]

$$n_{TiO_2}(\lambda) = \left(4.99 + \frac{1}{96.6\lambda^{1.1}} + \frac{1}{4.60\lambda^{1.95}}\right)^{1/2} \quad (2)$$

The wavelength-dependent refractive of the active material $MAPbI_3$ is taken from Refs. [34,35]. The optical response of indium tin oxide (ITO) nanocrystalline films and fluorine indium co-doped cadmium oxide (FICO) nanocrystalline films has been simulated by employing the Drude model and the effective medium approximation [36]. The filling factor of the ITO and FICO nanocrystalline films is 0.65. For ITO, $N = 2.49 \times 10^{26}$ cm^{-3}, $\varepsilon_\infty = 4$, $m^* = 0.4\ m_e$, and $\Gamma = 0.1132$ eV [24]. For FICO, $N = 1.68 \times 10^{27}$ cm^{-3}, $\varepsilon_\infty = 5.6$, $m^* = 0.43\ m_e$, and $\Gamma = 0.07$ eV [24,37].

3. Results

In Figure 1, a sketch of the $MAPbI_3$ metal halide perovskite light-emitting transistor, coupled with a microcavity, is shown. In such a structure, the thickness of the $MAPbI_3$ layer is 40 nm, the thickness of the ITO layers is 100 nm, the thickness of the FICO nanocrystalline layers is 112.7 nm, the thickness of the SiO_2 layers is 144.15 nm, and the thickness of the TiO_2 layers is 73.5 nm. The design of the device follows the sequence (from bottom to top) of ITO/(TiO_2/FICO)$_4$/SiO_2/$MAPbI_3$/SiO_2/ITO/(FICO/TiO_2)$_4$/ITO. In Figure 1, the white spaces in the photonic crystal represent the repetition of the TiO_2/FICO unit cell.

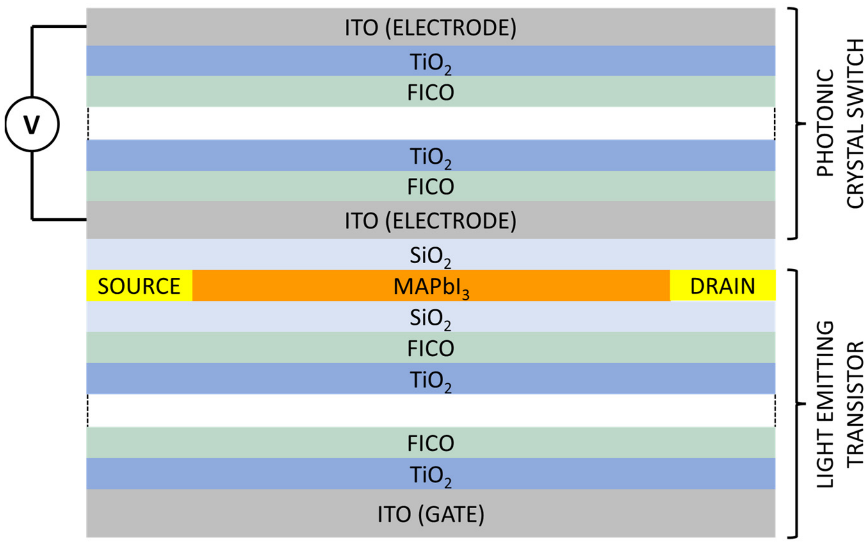

Figure 1. Sketch of the light-emitting transistor integrated with a microcavity in which the upper photonic crystal is a tunable switch activated by an external voltage. The sequence of the structure (from bottom to top) is ITO/(TiO_2/FICO)$_4$/SiO_2/$MAPbI_3$/SiO_2/ITO/(FICO/TiO_2)$_4$/ITO. The white spaces in the photonic crystal represent the repetition of the TiO_2/FICO unit cell.

The photonic crystal below the $MAPbI_3$ layer, made by TiO_2 and FICO nanocrystals, functions as a gate dielectric. Instead, the photonic crystal above the $MAPbI_3$ layer is made by TiO_2 and FICO nanoparticle layers sandwiched between two transparent electrodes of ITO and functions as electro-optic switch.

The application of an external voltage between the two ITO electrodes leads to a change in the carrier density of the doped semiconductor nanocrystals, i.e., FICO nanocrystals, resulting in a change in the dielectric function of the FICO nanoparticle layers and, thus, to a change in the effective refractive index of the photonic crystal. Such an effective refractive index change gives rise to a shift of the photonic band gap of the photonic crystal [26,38]. Referring to the structure sketched in Figure 1, the shift of the photonic band gap of the photonic crystal above the $MAPbI_3$ layer results in a modification of the light transmission spectrum of the light-emitting transistor coupled with the microcavity. In Figure 2, the transmission spectrum of the light-emitting transistor coupled with the microcavity is shown for two different carrier densities of the FICO nanocrystals: the solid black curve corresponds to the structure with a FICO carrier density of 1.68×10^{27} charges/m^3, while the dotted/dashed red curve corresponds to a FICO carrier density of 3.68×10^{27} charges/m^3.

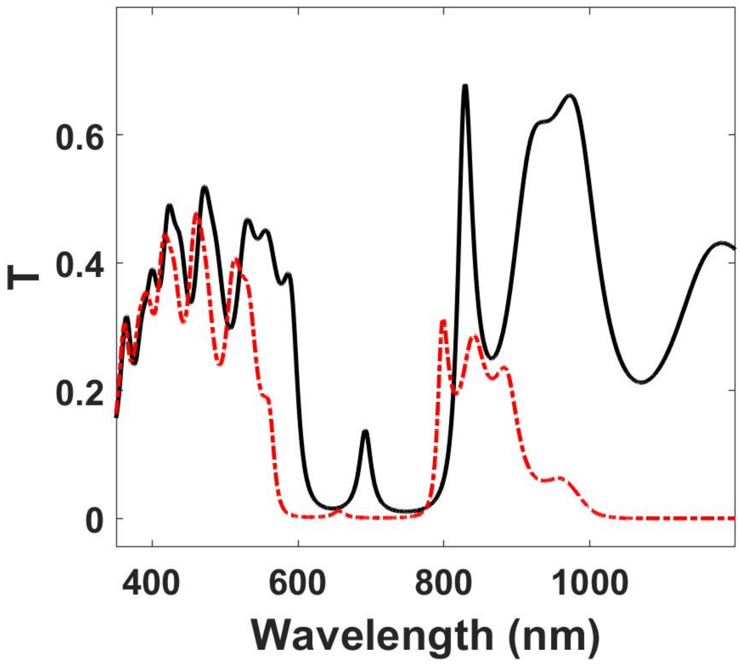

Figure 2. Transmission spectrum of the light-emitting transistor coupled with a tunable microcavity (structure depicted in Figure 1). The solid black curve corresponds to the structure with a FICO carrier density of 1.68×10^{27} charges/m^3, while the dotted/dashed red curve corresponds to a FICO carrier density of 3.68×10^{27} charges/m^3.

With such a change in carrier density of FICO nanocrystals, it is possible to almost completely suppress the defect mode of the microcavity. This is mainly due to the asymmetry generated between the two photonic crystals of the microcavities, i.e., the one below the $MAPbI_3$ layer and the one above the $MAPbI_3$ layer. To highlight the possibility of tuning the defect mode of the microcavity, in Figure 3, the transmission spectrum of the light-emitting transistor coupled with the microcavity is shown for six different carrier densities of the FICO nanocrystals: 1.68×10^{27} charges/m^3 (solid black curve), 1.88×10^{27} charges/m^3 (dotted/dashed red curve), 2.08×10^{27} charges/m^3 (dashed dark red curve), 2.28×10^{27} charges/m^3 (solid brown curve), 2.48×10^{27} charges/m^3 (dotted/dashed dark green curve), and 2.68×10^{27} charges/m^3 (dashed green curve). The arrow in the figure highlights the increase in carrier density.

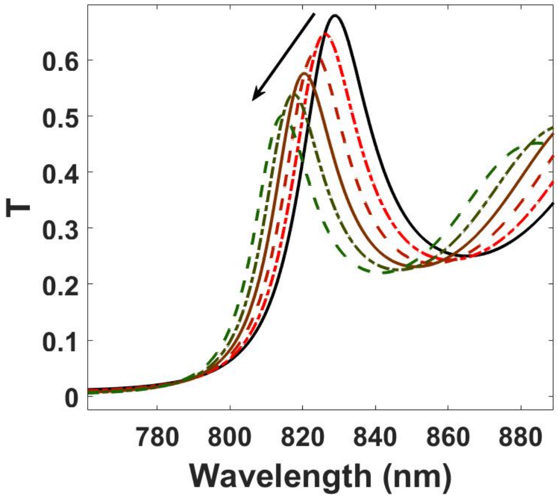

Figure 3. Transmission spectra of light-emitting transistor coupled with a tunable microcavity (structure depicted in Figure 1), in the spectral region of the defect mode, for a FICO carrier density of 1.68 × 10^{27} charges/m^3 (solid black curve), 1.88 × 10^{27} charges/m^3 (dotted/dashed red curve), 2.08 × 10^{27} charges/m^3 (dashed dark red curve), 2.28 × 10^{27} charges/m^3 (solid brown curve), 2.48 × 10^{27} charges/m^3 (dotted/dashed dark green curve), and 2.68 × 10^{27} charges/m^3 (dashed green curve). The arrow in the figure highlights the increase in carrier density.

A shift of about 20 nm is shown. With a simple linear fit, it is possible to determine that 7.2 × 10^{25} charges/m^3 are needed for a shift of 1 nm of the defect mode. In a similar photonic structure, i.e., a photonic crystal made with indium tin oxide and titanium dioxide layers, a shift of 23 nm has been achieved with an external voltage of 10 V [38]. Considering the electroluminescence (EL) of a light-emitting transistor based on $MAPbI_3$ (the experimental data were taken from Ref. [16]), it is possible to finely tune the EL by changing the FICO nanocrystal carrier density (Figure 4). As in Figure 3, the arrow underlines the increase in carrier density. Taking into account the aforementioned result for a similar photonic structure reported in Ref. [38], the EL shift (in nm) over the external voltage (in V) can be estimated for this transistor and the value is about 2 nm/V.

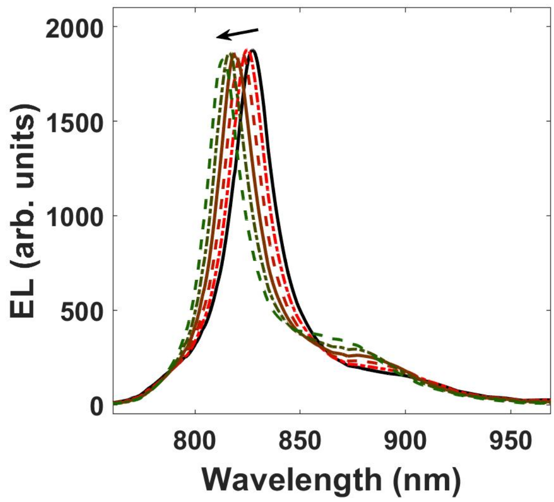

Figure 4. Electroluminescence (EL) of the metal halide perovskite light-emitting transistor/microcavity for a FICO carrier density of 1.68 × 10^{27} charges/m^3 (solid black curve), 1.88 × 10^{27} charges/m^3 (dotted/dashed red curve), 2.08 × 10^{27} charges/m^3 (dashed dark red curve), 2.28 × 10^{27} charges/m^3 (solid brown curve), 2.48 × 10^{27} charges/m^3 (dotted/dashed dark green curve), and 2.68 × 10^{27} charges/m^3 (dashed green curve). The arrow in the figure highlights the increase in carrier density.

An extension of this work could take into account an improvement in the performance, in terms of electroluminescence, of the light-emitting transistor through direct contact between a plasmonic material and the emitting material in the transistor, i.e., metal halide perovskite in this work. To study this possible improvement in transistor performance, very precise microscopic theories have been proposed for similar devices [39,40]. Such microscopic theories would allow the device and its characteristics to be studied with great accuracy.

4. Conclusions

In this work, the tunability, via the application of an external voltage, of the defect mode of the microcavity combined with a metal halide perovskite light-emitting transistor has been studied. In this way, the electroluminescence of the metal halide perovskite active layer can be modulated with an electric field. This tunability can be very interesting for lighting applications with tunable electrically stimulated light emitters. Since the integration of a microcavity in a light-emitting transistor can lead to a possible electrically injected metal halide perovskite laser, the device presented in this work can be interesting also for the realization of tunable lasers.

Funding: The author acknowledges the Research and Innovation Staff Exchange program SONAR (Marie Curie Actions) of the European Union's Horizon 2020 (Grant number 734690). This project has received funding from the European Research Council (ERC) under the European Union's Horizon 2020 research and innovation programme (grant agreement No. 816313).

Data Availability Statement: The data are available upon request to the author.

Conflicts of Interest: The author declares no conflict of interest.

References

1. Genco, A.; Mariano, F.; Carallo, S.; Guerra, V.L.P.; Gambino, S.; Simeone, D.; Listorti, A.; Colella, S.; Gigli, G.; Mazzeo, M. Fully Vapor-Deposited Heterostructured Light-Emitting Diode Based on Organo-Metal Halide Perovskite. *Adv. Electron. Mater.* **2016**, *2*, 1500325. [CrossRef]
2. Stranks, S.D.; Snaith, H.J. Metal-Halide Perovskites for Photovoltaic and Light-Emitting Devices. *Nat. Nanotechnol.* **2015**, *10*, 391–402. [CrossRef]
3. Elkhouly, K.; Gehlhaar, R.; Genoe, J.; Heremans, P.; Qiu, W. Perovskite Light Emitting Diode Characteristics: The Effects of Electroluminescence Transient and Hysteresis. *Adv. Opt. Mater.* **2020**, *8*, 2000941. [CrossRef]
4. Liu, A.; Bi, C.; Guo, R.; Zhang, M.; Qu, X.; Tian, J. Electroluminescence Principle and Performance Improvement of Metal Halide Perovskite Light-Emitting Diodes. *Adv. Opt. Mater.* **2021**, *9*, 2002167. [CrossRef]
5. Park, M.-H. 3D and 2D Metal Halide Perovskites for Blue Light-Emitting Diodes. *Materials* **2022**, *15*, 4571. [CrossRef] [PubMed]
6. Kim, G.-W.; Petrozza, A. Defect Tolerance and Intolerance in Metal-Halide Perovskites. *Adv. Energy Mater.* **2020**, *10*, 2001959. [CrossRef]
7. Kim, J.Y.; Lee, J.-W.; Jung, H.S.; Shin, H.; Park, N.-G. High-Efficiency Perovskite Solar Cells. *Chem. Rev.* **2020**, *120*, 7867–7918. [CrossRef]
8. Jeong, M.; Choi, I.W.; Go, E.M.; Cho, Y.; Kim, M.; Lee, B.; Jeong, S.; Jo, Y.; Choi, H.W.; Lee, J.; et al. Stable Perovskite Solar Cells with Efficiency Exceeding 24.8% and 0.3-V Voltage Loss. *Science* **2020**, *369*, 1615–1620. [CrossRef]
9. Wu, X.; Li, B.; Zhu, Z.; Chueh, C.-C.; Jen, A.K.-Y. Designs from Single Junctions, Heterojunctions to Multijunctions for High-Performance Perovskite Solar Cells. *Chem. Soc. Rev.* **2021**, *50*, 13090–13128. [CrossRef]
10. Jacobsson, T.J.; Hultqvist, A.; García-Fernández, A.; Anand, A.; Al-Ashouri, A.; Hagfeldt, A.; Crovetto, A.; Abate, A.; Ricciardulli, A.G.; Vijayan, A.; et al. An Open-Access Database and Analysis Tool for Perovskite Solar Cells Based on the FAIR Data Principles. *Nat. Energy* **2022**, *7*, 107–115. [CrossRef]
11. Fakharuddin, A.; Gangishetty, M.K.; Abdi-Jalebi, M.; Chin, S.-H.; bin Mohd Yusoff, A.R.; Congreve, D.N.; Tress, W.; Deschler, F.; Vasilopoulou, M.; Bolink, H.J. Perovskite Light-Emitting Diodes. *Nat. Electron.* **2022**, *5*, 203–216. [CrossRef]
12. Li, H.; Lin, H.; Ouyang, D.; Yao, C.; Li, C.; Sun, J.; Song, Y.; Wang, Y.; Yan, Y.; Wang, Y.; et al. Efficient and Stable Red Perovskite Light-Emitting Diodes with Operational Stability >300 h. *Adv. Mater.* **2021**, *33*, 2008820. [CrossRef] [PubMed]
13. Guo, B.; Lai, R.; Jiang, S.; Zhou, L.; Ren, Z.; Lian, Y.; Li, P.; Cao, X.; Xing, S.; Wang, Y.; et al. Ultrastable Near-Infrared Perovskite Light-Emitting Diodes. *Nat. Photon.* **2022**, *16*, 637–643. [CrossRef]
14. Chin, X.Y.; Cortecchia, D.; Yin, J.; Bruno, A.; Soci, C. Lead Iodide Perovskite Light-Emitting Field-Effect Transistor. *Nat. Commun.* **2015**, *6*, 7383. [CrossRef] [PubMed]
15. Lin, Y.-H.; Pattanasattayavong, P.; Anthopoulos, T.D. Metal-Halide Perovskite Transistors for Printed Electronics: Challenges and Opportunities. *Adv. Mater.* **2017**, *29*, 1702838. [CrossRef] [PubMed]

16. Maddalena, F.; Chin, X.Y.; Cortecchia, D.; Bruno, A.; Soci, C. Brightness Enhancement in Pulsed-Operated Perovskite Light-Emitting Transistors. *ACS Appl. Mater. Interfaces* **2018**, *10*, 37316–37325. [CrossRef] [PubMed]
17. Liu, Y.; Chen, P.-A.; Hu, Y. Recent Developments in Fabrication and Performance of Metal Halide Perovskite Field-Effect Transistors. *J. Mater. Chem. C* **2020**, *8*, 16691–16715. [CrossRef]
18. Klein, M.; Li, J.; Bruno, A.; Soci, C. Co-Evaporated Perovskite Light-Emitting Transistor Operating at Room Temperature. *Adv. Electron. Mater.* **2021**, *7*, 2100403. [CrossRef]
19. Klein, M.; Wang, Y.; Tian, J.; Ha, S.T.; Paniagua-Domínguez, R.; Kuznetsov, A.I.; Adamo, G.; Soci, C. Polarization-Tunable Perovskite Light-Emitting Metatransistor. *Adv. Mater.* **2023**, *35*, 2207317. [CrossRef]
20. Namdas, E.B.; Hsu, B.B.Y.; Yuen, J.D.; Samuel, I.D.W.; Heeger, A.J. Optoelectronic Gate Dielectrics for High Brightness and High-Efficiency Light-Emitting Transistors. *Adv. Mater.* **2011**, *23*, 2353–2356. [CrossRef]
21. Soldano, C. Engineering Dielectric Materials for High-Performance Organic Light Emitting Transistors (OLETs). *Materials* **2021**, *14*, 3756. [CrossRef] [PubMed]
22. Scotognella, F. Microcavities Integrated in Metal Halide Perovskite Light-Emitting Field-Effect Transistors. *Res. Phys.* **2022**, *44*, 106168. [CrossRef]
23. Luther, J.M.; Jain, P.K.; Ewers, T.; Alivisatos, A.P. Localized Surface Plasmon Resonances Arising from Free Carriers in Doped Quantum Dots. *Nat. Mater.* **2011**, *10*, 361–366. [CrossRef]
24. Kriegel, I.; Scotognella, F.; Manna, L. Plasmonic Doped Semiconductor Nanocrystals: Properties, Fabrication, Applications and Perspectives. *Phys. Rep.* **2017**, *674*, 1–52. [CrossRef]
25. Agrawal, A.; Johns, R.W.; Milliron, D.J. Control of Localized Surface Plasmon Resonances in Metal Oxide Nanocrystals. *Ann. Rev. Mater. Res.* **2017**, *47*, 1–31. [CrossRef]
26. Paternò, G.M.; Moscardi, L.; Kriegel, I.; Scotognella, F.; Lanzani, G. Electro-Optic and Magneto-Optic Photonic Devices Based on Multilayer Photonic Structures. *J. Photon. Energy* **2018**, *8*, 032201. [CrossRef]
27. Born, M.; Wolf, E.; Bhatia, A.B.; Clemmow, P.C.; Gabor, D.; Stokes, A.R.; Taylor, A.M.; Wayman, P.A.; Wilcock, W.L. *Principles of Optics: Electromagnetic Theory of Propagation, Interference and Diffraction of Light*, 7th ed.; Cambridge University Press: Cambridge, MA, USA, 1999; ISBN 978-0-521-64222-4.
28. Xiao, X.; Wenjun, W.; Shuhong, L.; Wanquan, Z.; Dong, Z.; Qianqian, D.; Xuexi, G.; Bingyuan, Z. Investigation of Defect Modes with Al2O3 and TiO2 in One-Dimensional Photonic Crystals. *Optik* **2016**, *127*, 135–138. [CrossRef]
29. Lova, P.; Manfredi, G.; Comoretto, D. Advances in Functional Solution Processed Planar 1D Photonic Crystals. *Adv. Opt. Mater.* **2018**, *6*, 1800730. [CrossRef]
30. Nayak, C.; Bezerra, C.G.; Costa, C.H. Photonic Transmission Spectra in Graphene-Based Gaussian Random Multilayers. *Opt. Mater.* **2020**, *104*, 109838. [CrossRef]
31. Malitson, I.H. Interspecimen Comparison of the Refractive Index of Fused Silica. *J. Opt. Soc. Am. JOSA* **1965**, *55*, 1205–1209. [CrossRef]
32. RefractiveIndex.INFO—Refractive Index Database. Available online: https://refractiveindex.info/ (accessed on 15 November 2019).
33. Scotognella, F.; Chiasera, A.; Criante, L.; Aluicio-Sarduy, E.; Varas, S.; Pelli, S.; Łukowiak, A.; Righini, G.C.; Ramponi, R.; Ferrari, M. Metal Oxide One Dimensional Photonic Crystals Made by RF Sputtering and Spin Coating. *Ceram. Int.* **2015**, *41*, 8655–8659. [CrossRef]
34. Phillips, L.J.; Rashed, A.M.; Treharne, R.E.; Kay, J.; Yates, P.; Mitrovic, I.Z.; Weerakkody, A.; Hall, S.; Durose, K. Dispersion Relation Data for Methylammonium Lead Triiodide Perovskite Deposited on a (100) Silicon Wafer Using a Two-Step Vapour-Phase Reaction Process. *Data Brief* **2015**, *5*, 926–928. [CrossRef] [PubMed]
35. Phillips, L.J.; Rashed, A.M.; Treharne, R.E.; Kay, J.; Yates, P.; Mitrovic, I.Z.; Weerakkody, A.; Hall, S.; Durose, K. Maximizing the Optical Performance of Planar $CH_3NH_3PbI_3$ Hybrid Perovskite Heterojunction Stacks. *Sol. Energy Mater. Sol. Cells* **2016**, *147*, 327–333. [CrossRef]
36. Paternò, G.M.; Iseppon, C.; D'Altri, A.; Fasanotti, C.; Merati, G.; Randi, M.; Desii, A.; Pogna, E.A.A.; Viola, D.; Cerullo, G.; et al. Solution Processable and Optically Switchable 1D Photonic Structures. *Sci. Rep.* **2018**, *8*, 3517. [CrossRef] [PubMed]
37. Kriegel, I.; Urso, C.; Viola, D.; De Trizio, L.; Scotognella, F.; Cerullo, G.; Manna, L. Ultrafast Photodoping and Plasmon Dynamics in Fluorine–Indium Codoped Cadmium Oxide Nanocrystals for All-Optical Signal Manipulation at Optical Communication Wavelengths. *J. Phys. Chem. Lett.* **2016**, *7*, 3873–3881. [CrossRef]
38. Moscardi, L.; Paternò, G.M.; Chiasera, A.; Sorrentino, R.; Marangi, F.; Kriegel, I.; Lanzani, G.; Scotognella, F. Electro-Responsivity in Electrolyte-Free and Solution Processed Bragg Stacks. *J. Mater. Chem. C* **2020**, *8*, 13019–13024. [CrossRef]
39. Jacak, W.A. *Quantum Nano-Plasmonics*, 1st ed.; Cambridge University Press: Cambridge, MA, USA, 2020; ISBN 978-1-108-77769-8.
40. Laska, M.; Krzemińska, Z.; Kluczyk-Korch, K.; Schaadt, D.; Popko, E.; Jacak, W.A.; Jacak, J.E. Metallization of Solar Cells, Exciton Channel of Plasmon Photovoltaic Effect in Perovskite Cells. *Nano Energy* **2020**, *75*, 104751. [CrossRef]